Report Summer School at Fermilab

Impact of a track trigger
at a multi-TeV muon collider

Giulia Liberalato

September 2022

Contents

Abstract **0**

1 Introduction to Muon Collider **2**
1.1 Why, Who, Where, When 2
1.2 Benefits of Muon Collider 4
1.3 BIB challenge 5
1.4 Detector 6

2 Physics processes **8**
2.1 Strategy of work 8
2.2 Event generation with MadGraph 9

3 My analyses with CERN-ROOT and trigger strategy **12**
3.1 H analysis 12
3.2 Efficiency analysis 14
3.3 Number of events analysis 16

Conclusion **19**

Appendix 1 **20**

Appendix 2 **30**

Bibliography **40**

Abstract

In the panorama of future particle accelerators, the Muon Collider seems to be the best choice for several reasons that will be explored in section 1.2. The main challenge is represented by the instability of the muons. At the desired instantaneous luminosities, an intense flow of secondary and tertiary particles from the interactions of the beam decay products with the machine elements reaches the detector, compromising its performance. Several studies are currently underway to mitigate the background and to have an efficient trigger. My work represents a first step towards understanding the basic characteristics of a trigger selection, which will subsequently guide the design of the trigger system. With this aim I produced and analyzed Higgs and di-Higgs signals with MadGraph and CERN-ROOT.

In first section there is an introduction to Muon Collider, a brief history, a discussion of its benefits, a description of the detector and of the effectsof the Beam Induced Background. Several operating center-of-mass energies are possible for this machine, in this report a center-of-mass of 3 TeV is assumed. Then I describe the event generation process. Finally I describe the entire analysis, in particular I analyzed the efficiency and the number of events for each process.

1 Introduction to Muon Collider

The Standard Model (SM) of particle physics has been a highly successful theory for describing measurements at the energy frontier. However, observations and theoretical motivations indicate the presence of physical phenomena Beyond the Standard Model (BSM). Experimental detection of such phenomena, in most cases, require higher energies than those currently accessible. The most probable energy regime in which BSM phenomena would occur are at energy scales of few TeVs. In the landscape of possible future energy frontier accelerators, a circular muon collider is a particularly interesting option for the future of energy frontier exploration.

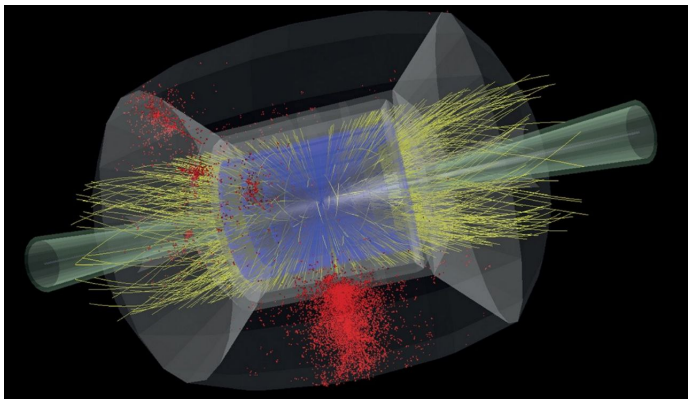

Figure 1: Muon Collider.

1.1 Why, Who, Where, When

The concept of a muon collider is not new. In the 1990s, a muon collider collaboration was formed in the United States. In 2000, the Neutrino Factory and Muon Collider Collaboration (NFMCC) was formed which set out to run a multi-year research and development program aimed at validating critical design concepts for the Neutrino Factory (NF) and Muon Collider (MC). The Muon Accelerator Program (MAP) was a program approved in 2011 and instructed to evaluate the feasibility of the technologies required for the construction of the NF and MC. Since 2011, the muon collider is attracting increasing interest from the scientific community, and despite the activities of MAP were suspended in 2016, several design and feasibility studies resulted in the muon collider being considered a promising project, although still immature, compliant with all the criteria established for future colliders by the 2020 update of the European Strategy for Particle Physics. Currently, many research groups from laboratories all around the world are forming a new international collaboration to develop the muon collider project as the next energy-frontier-exploration machine. CERN formed a new Interna-

tional Muon Collider Collaboration (IMCC) to assess feasibility of building a high energy muon collider, identify critical challenges, and develop an R & D program aimed to address them. The effort includes development of the machine-detector interface, detector concepts, and an evaluation of the physics potential.

About the place where MC can be built there are two options: Fermilab or CERN. The idea of having a MC as a potential “site filler" for Fermilab dates back to the early 2000's, when parameters for a 4 TeV machine were presented. More recently, using higher field magnets and higher-gradient acceleration, the parameter space towards a 10 TeV Muon Collider concept that would fit within the Fermilab site has been identified and a first design concept has been developed. A schematic layout of this configuration is shown in Figure 2. The concept begins with use of PIP-II as the initial part of the proton source [1].

Figure 2: A schematic view of the Fermilab site and the layout of a possible complex for the Muon Collider site-filler.

For the second option, a preliminary study of a center-of-mass 14 TeV Muon Collider in the CERN LHC tunnel has recently been considered. It leverages the existing CERN facilities, including the 26.7 km circumference LHC tunnel and its injectors [2].

In figure 3 we can see next steps of Muon Collider program, the timeline shows the plan divided by source and collider complex, cooling demonstrator and hardware.

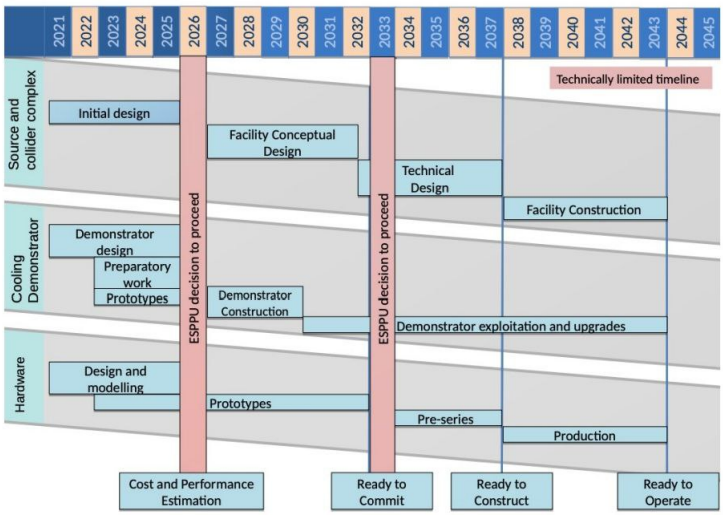

Figure 3: Muon Collider timeline.

1.2 Benefits of Muon Collider

Future high-energy particle physics facilities have been evaluated on the basis of these criteria: scientific potential, technical construction and financial requirements and flexibility for further upgrades and developments. The European Strategy for Particle Physics has added an important new requirement: next-generation facilities should meet very high ecological and environmental standards and, in particular, should be energy efficient [3]. Physics need multi-TeV colliders to push forward the frontier of knowledge to shed light onto many open questions, the FCC (Future Circular Collider) has been proposed to reach the center-of-mass-energy of 100 TeV colliding protons and to achieve this goal. On the other hand, muons can probe much higher energy scales than protons colliding with the same beam energy because the energy of proton is distributed among its constituent quarks and gluons, whereas muons are leptons, elementary particles.

Compared to circular electron-positron accelerators, muons are 200 times havier than electrons, so the advantage of colliding muons is that they can be accelerated in rings without suffering from the large synchrotron radiation losses that limit the performance of electron–positron colliders. This is explained by the Larmor formula multiplied by the fourth power of the Lorentz factor, we see the power that relativistically moving particles radiate in a torus around the acceleration vector is:

$$P = \frac{1}{6\pi\varepsilon_0}\frac{e^2}{c^3}\frac{v^2}{r^2}\left(\frac{E}{m}\right)^4, \tag{1}$$

where v is the particle speed of mass m and energy E, r is the radius of the

accelerator, e the elementary charge and ε_0 the dielectric constant in vacuum. We note the inverse proportionality from the fourth power of the mass and therefore it can be deduced that muons, being more massive, radiate less than electrons [4].

An important feature of particle accelerators is the luminosity which is defined as:

$$L = \frac{1}{\sigma}\frac{dN}{dt} \ , \tag{2}$$

where σ is the cross section of a process and dN is the number of events produced in the period of time dt. Therefore accelerators with high luminosity can reveal rare phenomena, namely those with a low cross section. Figure 4 shows energy efficiency of present and future colliders, the annual integrated luminosity ($1\ \text{ab} = 10^{-42}\ \text{cm}^2$) per terawatt hour of electric power consumption as a function of the centre-of-mass energy: as you can see the Muon Collider would exceed the energy of $\sqrt{s} = 10$ TeV with a good efficiency, because this increases as the energy of the center of mass increases. Considering energies above $\sqrt{s} = 2$ TeV the Muon Collider would prove to be the most efficient choice for exploring high energy levels [3].

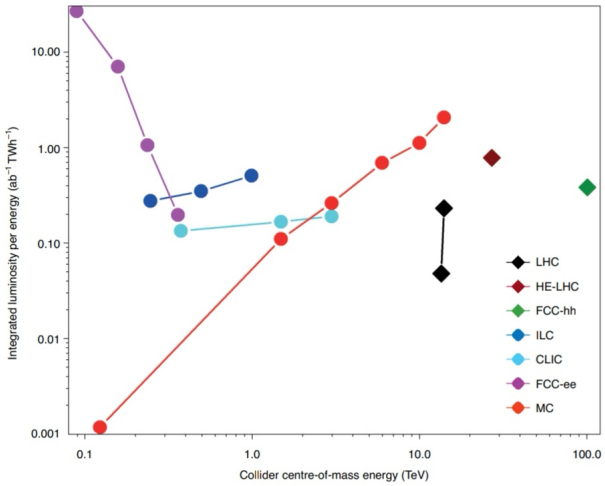

Figure 4: Energy efficiency of present and future colliders [3].

1.3 BIB challenge

Beam Induced Background (BIB) is identified as one of the main challenges of Muon Collider, it is a continuous flux of secondary and tertiary particles produced by the muon decays and their interaction with the machine elements. In fact muons are unstable particles and they decay with an average

lifetime of $\tau_\mu = 2.2$ μs at rest. The detectors and event reconstruction techniques need to be designed to cope with the presence of the BIB because it degrades the performance of detector. The expected characteristics of BIB depend on the beam properties, accelerator lattice, interaction region and from detector design. Detailed simulation studies have been performed using the MARS15 software and a combination of Linebuilder and FLUKA. In particular, these studies were performed for a collider with center-of-mass energy of 1.5 TeV. BIB properies are shown in figure 5 and we can see that they are low-momentum particles, partially out-of-time with respect to the bunch crossing. FLUKA simulations at $\sqrt{s} = 3$ TeV and $\sqrt{s} = 10$ TeV are currently under development, but the preliminary results show a BIB with intensity of the same level as in the $\sqrt{s}$ =1.5 TeV configuration [1].

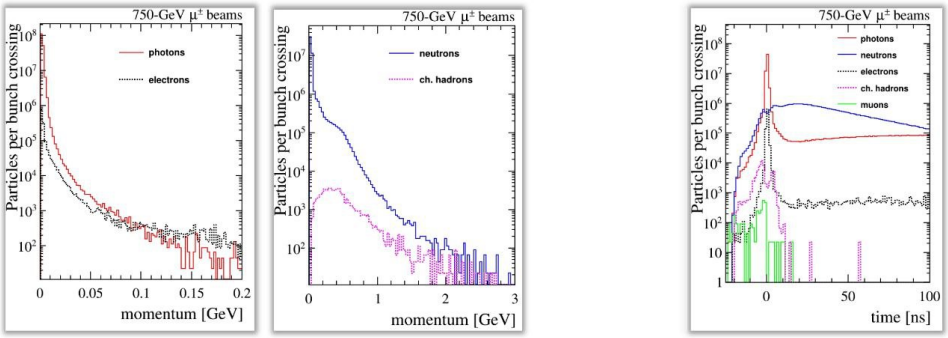

Figure 5: Remaining BIB properties [6].

1.4 Detector

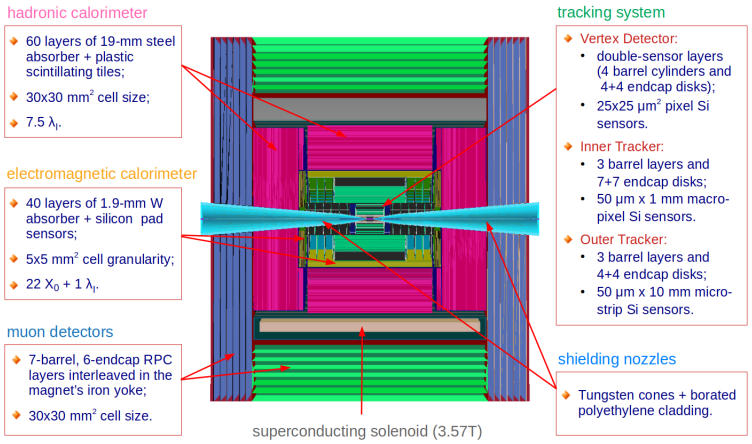

Figure 6: Schematic overview of the longitudinal section of the muon collider detector [7].

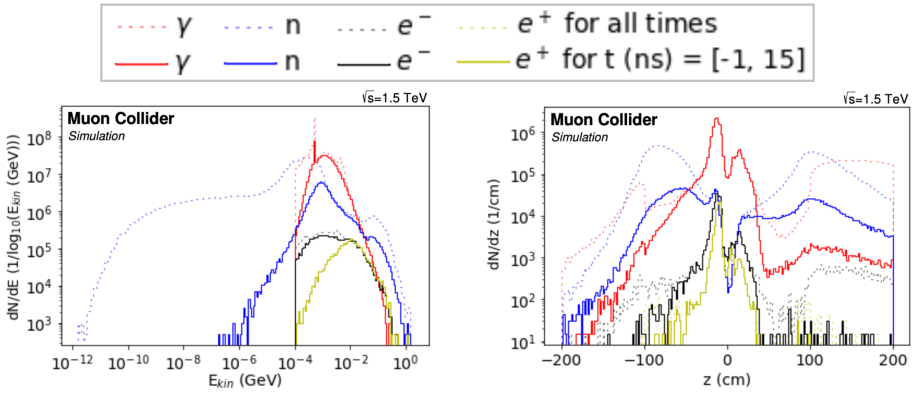

Figure 7: Kinetic energy plot (left) and longitudinal exit coordinate distribution (right) of BIB particles, divided by particle type. Results by FLUKA [5].

Particles from BIB can deposit a huge amount of energy in the detector, if not shielded properly. For this reason an essential part of the machine detector interface at a Muon Collider is a pair of tungsten nozzles (figure 6) which reduce the rate and energy of BIB particles reaching the detector by several orders of magnitude. Such a nozzle also limits the acceptance of the detector to polar angles $\theta > 10°$. The flux of particles surviving the shielding and entering the detector arise partially through shower products of BIB particles exiting the nozzle and through back-scattering of particles from one beam into the nozzle on the opposite side of the Interaction Point (IP) with respect to the direction the beam is arriving from. The result is a diffuse background of mostly low-momentum and out-of-time photons, neutrons, and electrons/positrons. The nozzles act in a very significant way in cutting out the high energy BIB component: as we can notice in figure 7 the BIB particles entering the detector hall have kinetic energy below few GeVs. Only charged hadrons and secondary muons can reach much higher energies but their number is quite low, in the order of 10^4 and 10^3 , with respect to 10^7 photons, neutrons and 10^5 electrons, positrons [5].

2 Physics processes

Measurements of the Higgs properties are a powerful probe of new physics, and they play a central role in the physics programs of all foreseen future colliders. Multi-TeV energies allow for the production of a large sample of Higgs bosons with a clean environment to study them. In addition, they allow multi-Higgs production and therefore an unmatched probe of the Higgs potential. Futhermore, high energy muon colliders offer the unique ability to simultaneously access Higgs properties with very high precision and accuracy, and in case of deviations, directly probe their origin.

During my work at Fermilab I considered the following processes.

- $\mu^+\mu^- \to h\ \nu_\mu\ \overline{\nu}_\mu\ ,\ h \to b\ \overline{b}$
- $\mu^+\mu^- \to h\ h\ \nu_\mu\ \overline{\nu}_\mu\ ,\ h \to b\ \overline{b}$
- $\mu^+\mu^- \to W^+\ W^-\ \nu_\mu\ \overline{\nu}_\mu\ ,\ W^- \to d\ \overline{u}$
- $\mu^+\mu^- \to W^+\ W^-\ \nu_\mu\ \overline{\nu}_\mu\ ,\ W^- \to s\ \overline{c}$

2.1 Strategy of work

Collisions in Muon Collider are expected to happen at the maximum rate of 100 kHz, corresponding to the minimum time between crossings of 10 μs. We need Trigger and Data Acquisition (TDAQ) systems to try to store only the events which are interesting from the point of view of the physics that we want to study. The amount of data acquired by the muon collider experiments is expected to be dominated by the tracker and calorimeters. For the silicon tracker, we estimate event size and data rates by acquiring an average number of hits per event from simulation and multiplying it by the 100 kHz event rate. We assume that each hit consists of 32 bits to encode charge, position, and time information and that zero-suppression is applied in the detector front-end. Hits are integrated in the time period of 1 ns following the bunch crossing, which allows to preserve good efficiency for hits from particles originating in the hard scattering but rejects a significant fraction of the BIB. The full data rate corresponding to the sum of the tracker and calorimeter rates is about 60 Tb/s, which is a factor of few larger than the high level trigger (HLT) input of LHCb experiment in Run-3 and comparable to HLT input of CMS experiment in HL-LHC. Therefore, from the data volumes point of view, a streaming operation at 100 kHz appears to be feasible. We want to study if we can have an efficient trigger based on the presence of one or more tracks above a certain PT threshold.

2.2 Event generation with MadGraph

The signal Monte Carlo (MC) samples are produced with the event generator MadGraph5 [8] aMC@NLO v3.1.0 for the generation of the hard scattering processes, and Pythia 8 [9] for the parton showering, hadronization and fragmentation of hadrons, and decays. The generation of all MC samples is performed with 10000 events at $\sqrt{s} = 3$ TeV, with luminosity of $L = 1ab^{-1}$, importing the full standard model and assuming Higgs boson with width $\Gamma_H = 4.07 \times 10^{-3}$ GeV. In Appendix 1 there are all Feynman diagrams made by MadGraph5, whereas below there is the most relevant diagram for each process, the one with the larger cross section.

- $\mu^+\mu^- \to h\ \nu_\mu\ \overline{\nu}_\mu\ ,\ h \to b\ \overline{b}$
  Cross-section: $\sigma = (0.5131 \pm 0.0012)$ pb
  This is the Feynman diagram of process with largest cross section, $\sigma = (0.4995 \pm 0.00117)$ pb.

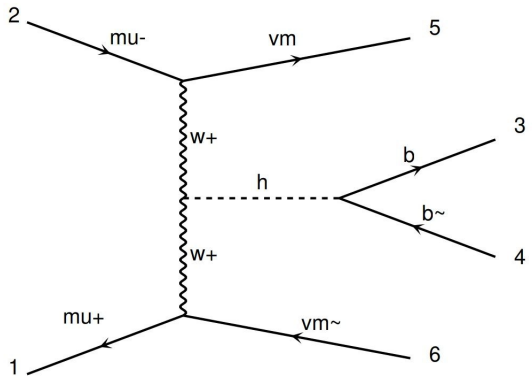

diagram 5 QCD=0, QED=4

- $\mu^+\mu^- \to h\ h\ \nu_\mu\ \overline{\nu}_\mu\ ,\ h \to b\ \overline{b}$
  Cross-section: $\sigma = (0.0009059 \pm 3.52 \times 10^{-6})$ pb
  This is the Feynman diagram of process with largest cross section, $\sigma = (0.0008405 \pm 3.46 \times 10^{-6})$ pb.

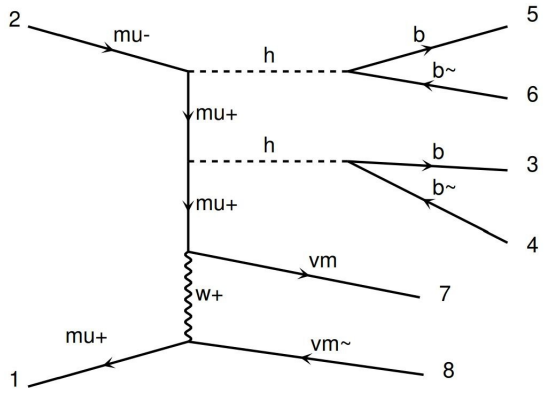

diagram 20 QCD=0, QED=6

- $\mu^+\mu^- \to W^+\, W^-\, \nu_\mu\, \overline{\nu}_\mu\ ,\ W^- \to d\, \overline{u}$
  Cross-section: $\sigma = (0.041224 \pm 0.000109)$ pb
  This is the Feynman diagram of process with largest cross section, $\sigma = (0.01644 \pm 7.03 \times 10^{-5})$ pb.

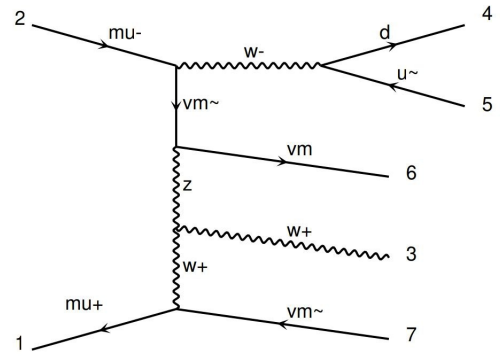

diagram 26 QCD=0, QED=5

- $\mu^+\mu^- \to W^+\, W^-\, \nu_\mu\, \overline{\nu}_\mu\ ,\ W^- \to s\, \overline{c}$
  Cross-section: $\sigma = (0.039079 \pm 0.000111)$ pb
  This is the Feynman diagram of process with largest cross section, $\sigma = (0.01562 \pm 6.47 \times 10^{-5})$ pb.

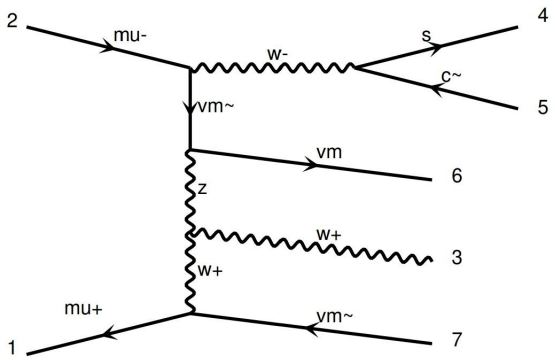

diagram 32 QCD=0, QED=5

3 My analyses with CERN-ROOT and trigger strategy

I analyzed Monte Carlo samples with Root, a software package for data analysis developed by CERN [10]. First of all I selected the charged particles in the final state based on their PID's, the charged-ones because they are the only one that we want to use for the trigger which is based on tracks. I found kaons (K), pions (π), protons (p), electrons (e) and muons (μ). I applied differents selections of θ: without cut the spherical coordinate θ is between 0° and 180°, the first cut is between 15° and 165° because the detector noozles stop particles in the first and last 15°. Finally I applied also a cut at 45° to see how much the efficiency change in this different region.

A common trigger strategy is to look for one or more tracks with a large transverse momentum (PT), as a first step in this direction I plot the fraction of events containing at least one track with a PT above a certain threshold. This would represent the efficiency of a single track trigger for a particular process as analyzed in section 3.2.

3.1 H analysis

For the process

$$\mu^+\mu^- \to h\ \nu_\mu\ \overline{\nu}_\mu\ ,\ h \to b\ \overline{b}$$

I saw the distributions of PT, spherical coordinates θ and φ and energy of each charged particle in final state (see Appendix 2) and then I considered all of them together as from figure 8 to figure 11.

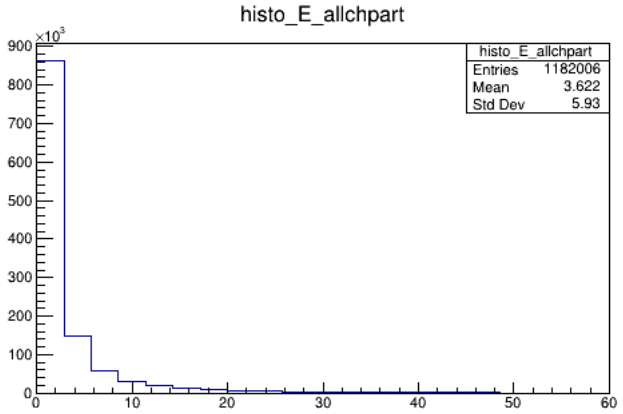

Figure 8: Energy distribution of all charged particles.

Then for each event I selected the particle with the greatest PT and I analyzed the number of tracks I have for each selection of polar angle region. The result is in figure 12.

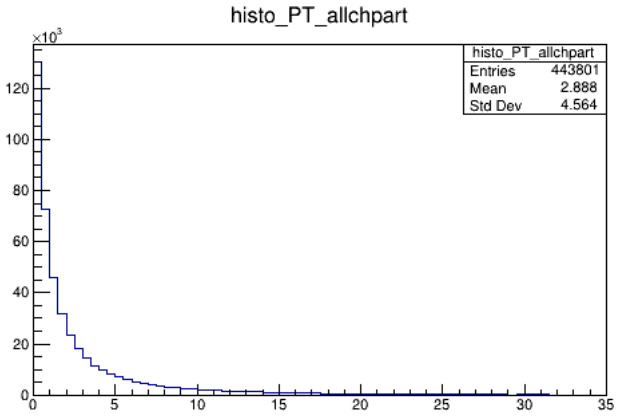

Figure 9: Transverse momentum distribution of all charged particles.

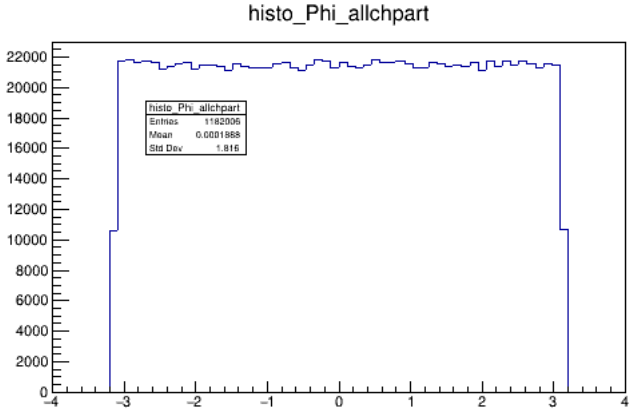

Figure 10: φ distribution of all charged particles.

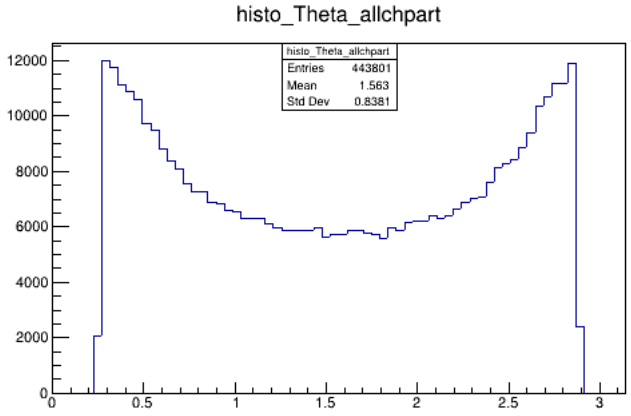

Figure 11: θ distribution of all charged particles.

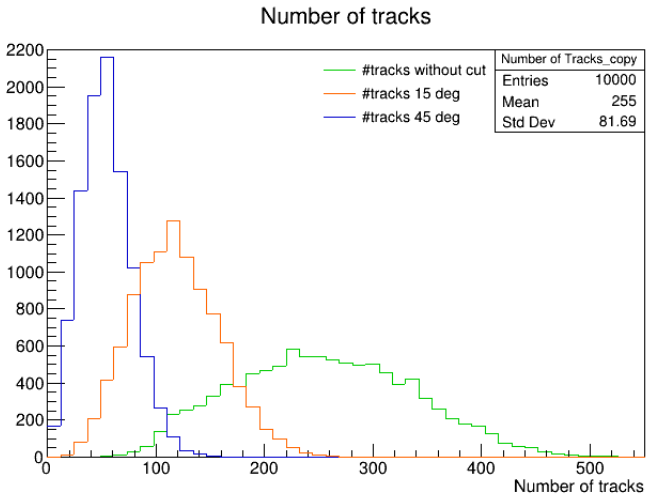

Figure 12: Number of tracks for differents polar angle regions.

With this plot I discovered that with the cut at 45° I have few events without particles in this region.

3.2 Efficiency analysis

For the efficiency analysis I plot the fraction of events containing at least one track with a PT above a certain threshold. This would represent the efficiency of a single track trigger for a particular process and I did this for every process generated with MadGraph. In figure 13 and 14 you can see the efficiency of

$$\mu^+\mu^- \to h\ \nu_\mu\ \overline{\nu}_\mu\ ,\ h \to b\ \overline{b}$$

and

$$\mu^+\mu^- \to h\ h\ \nu_\mu\ \overline{\nu}_\mu\ ,\ h \to b\ \overline{b}$$

The PT threshold is on the horizontal axis and there is only the first range in PT between 0 and 50 GeV. We have a good efficiency from 0 GeV to about 15-20 GeV for both full range of θ (green line) and for cut at 15° (orange line) while with a cut at 45° (blue line) we loose efficiency.

In figure 15 you can see a comparison between H and di-H signals: we can see that we have an higher efficiency for di-H process, for example at 5 GeV we have an efficiency of about 65% for H signal and about 85% for HH signal.

I did the same analysis also for processes

$$\mu^+\mu^- \to W^+\ W^-\ \nu_\mu\ \overline{\nu}_\mu\ ,\ W^- \to d\ \overline{u}$$

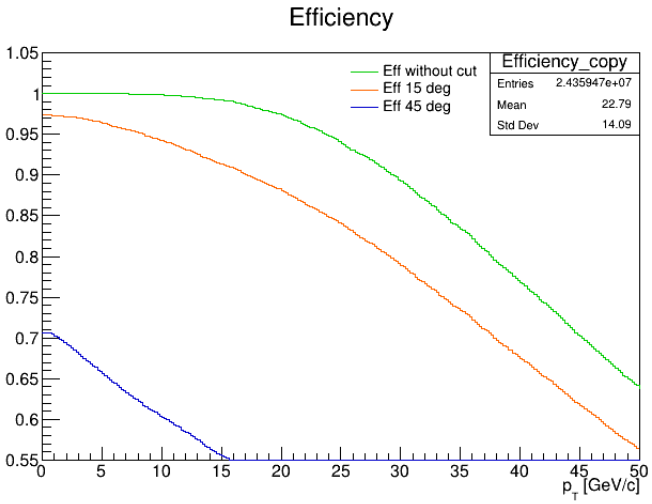

Figure 13: Efficiency for process $\mu^+\mu^- \to h\ \nu_\mu\ \overline{\nu}_\mu\ ,\ h \to b\ \overline{b}$.

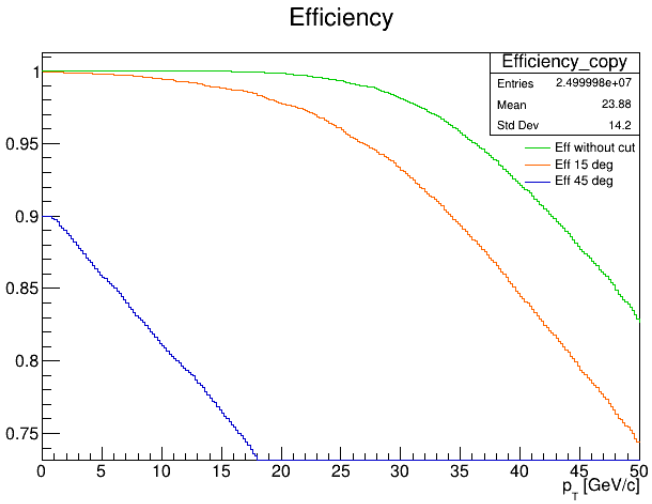

Figure 14: Efficiency for process $\mu^+\mu^- \to hh\ \nu_\mu\ \overline{\nu}_\mu\ ,\ h \to b\ \overline{b}$.

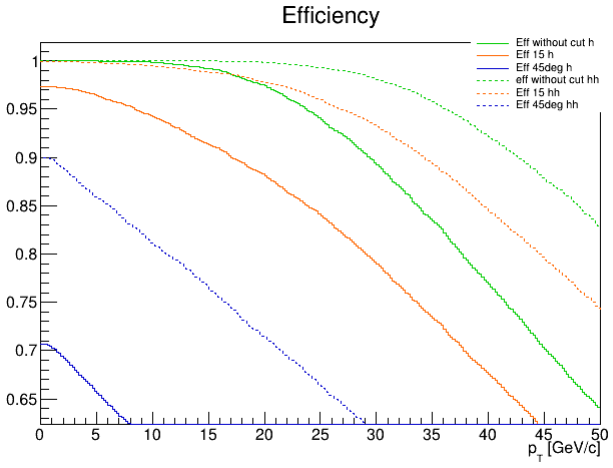

Figure 15: Efficiency for process $\mu^+\mu^- \to h\ \nu_\mu\ \overline{\nu}_\mu\ ,\ h \to b\ \overline{b}$ and $\mu^+\mu^- \to hh\ \nu_\mu\ \overline{\nu}_\mu\ ,\ h \to b\ \overline{b}$ together.

and

$$\mu^+\mu^- \to W^+\ W^-\ \nu_\mu\ \overline{\nu}_\mu\ ,\ W^- \to s\ \overline{c},$$

that are other important processes we can study with muon collider. In figure 16 there is the comparison in efficiency between these two processes.

3.3 Number of events analysis

After the efficiency analysis I analyzed the number of events as the efficiency for a certain PT threshold multiplied by the cross section given by MadGraph (as in section 2.2) and the integrated luminosity $L = 1\ ab^{-1}$ in 5 years (figures 17 and 18). The cross section for HH is smaller than for H, so the number of events is correspondently smaller.

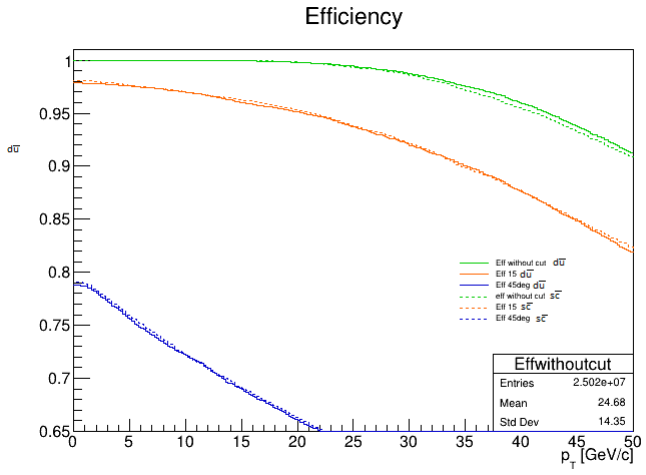

Figure 16: Efficiency for process $\mu^+\mu^- \to W^+\ W^-\ \nu_\mu\ \overline{\nu}_\mu\ ,\ W^- \to d\ \overline{u}$ and $\mu^+\mu^- \to W^+\ W^-\ \nu_\mu\ \overline{\nu}_\mu\ ,\ W^- \to s\ \overline{c}$ together.

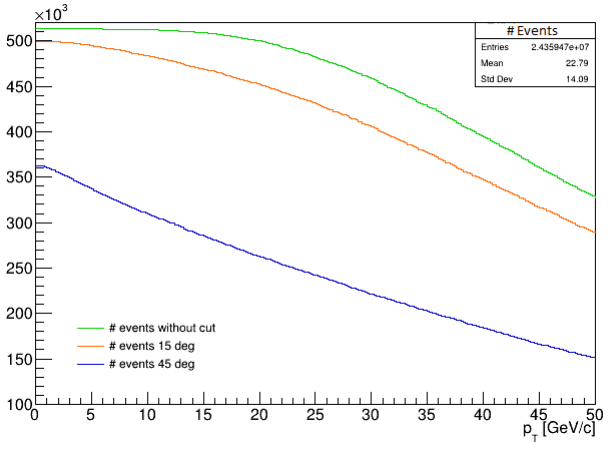

Figure 17: Number of events for process $\mu^+\mu^- \to h\ \nu_\mu\ \overline{\nu}_\mu\ ,\ h \to b\ \overline{b}$.

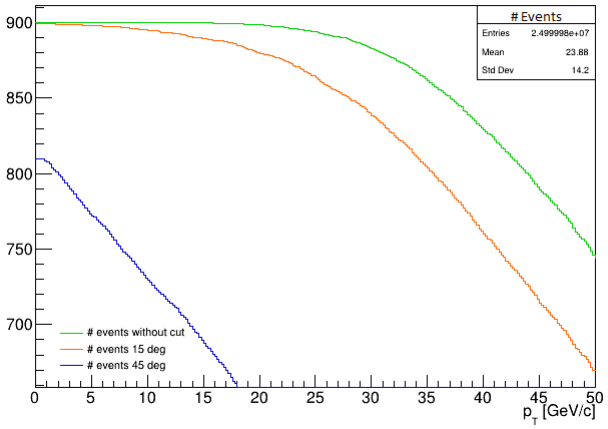

Figure 18: Number of events for process $\mu^+\mu^- \to hh\ \nu_\mu\ \overline{\nu}_\mu\ ,\ h \to b\ \overline{b}$.

Conclusion

The aim of my work was to study mainly the processes of Higgs and di-Higgs signals as a first step towards understanding the basic characteristics of a trigger selection, which will subsequently guide the design of the trigger system. My analysis focused on the study of the efficiency and number of events as functions of the transverse momentum PT. Efficiency is represented by the fraction of events containing at least one track with a PT above a certain threshold.

In the future it is important to continue studying the properties of the background, for now we know that BIB is mainly composed by low momentum particles and this is the reason why I studied the efficiency as a function of PT. Then from the comparison between signal and background properties we can hope to find an optimal PT threshold. Furthermore in this report I analyzed events generated with a center-of-mass energy of 3 TeV, but we are also planning to extend this study to 10 TeV.

Appendix 1

In this section there are all Feynman diagrams made by MadGraph5 for each process analyzed.

- $\mu^+\mu^- \to h\ \nu_\mu\ \overline{\nu}_\mu\ ,\ h \to b\ \overline{b}$

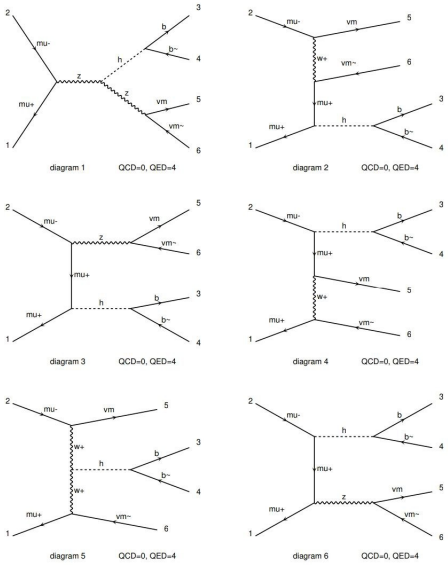

- $\mu^+\mu^- \to h\ h\ \nu_\mu\ \overline{\nu}_\mu\ ,\ h \to b\ \overline{b}$

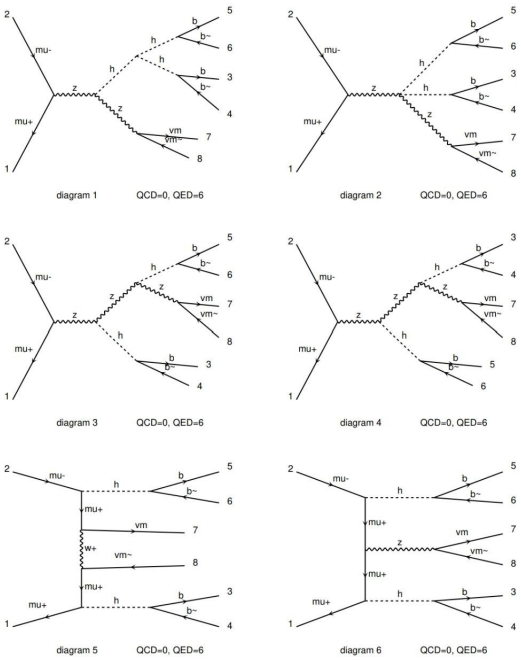

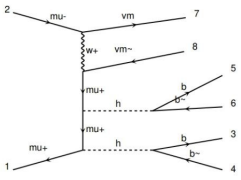

diagram 7 QCD=0, QED=6

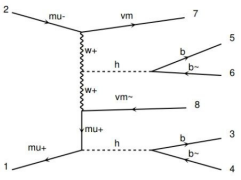

diagram 8 QCD=0, QED=6

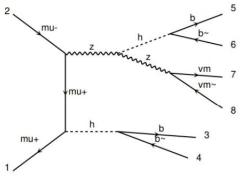

diagram 9 QCD=0, QED=6

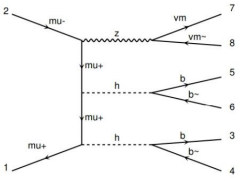

diagram 10 QCD=0, QED=6

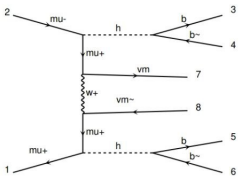

diagram 11 QCD=0, QED=6

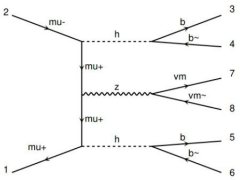

diagram 12 QCD=0, QED=6

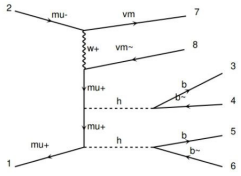

diagram 13 QCD=0, QED=6

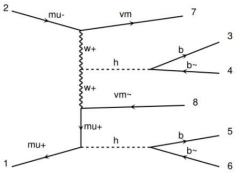

diagram 14 QCD=0, QED=6

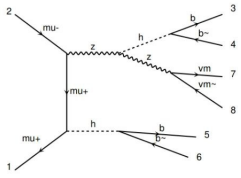

diagram 15 QCD=0, QED=6

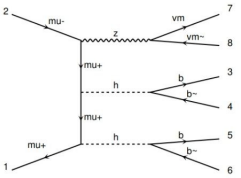

diagram 16 QCD=0, QED=6

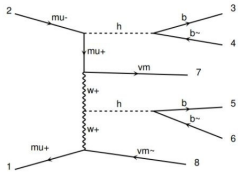

diagram 17 QCD=0, QED=6

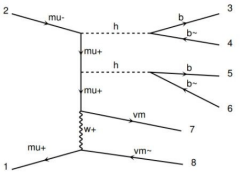

diagram 18 QCD=0, QED=6

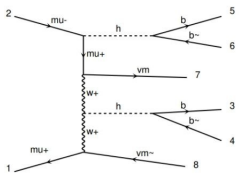

diagram 19 QCD=0, QED=6

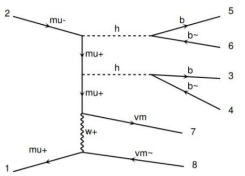

diagram 20 QCD=0, QED=6

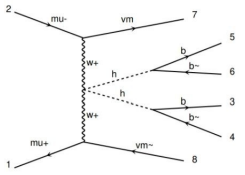

diagram 21 QCD=0, QED=6

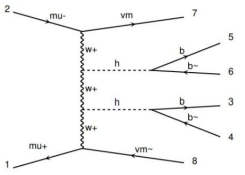

diagram 22 QCD=0, QED=6

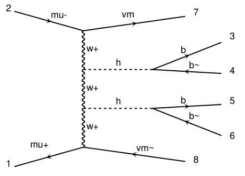

diagram 23 QCD=0, QED=6

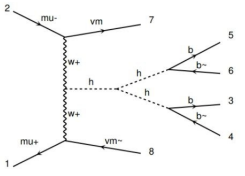

diagram 24 QCD=0, QED=6

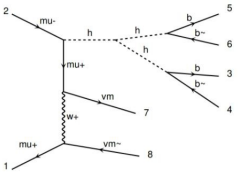

diagram 25 QCD=0, QED=6

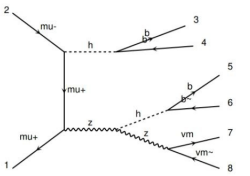

diagram 26 QCD=0, QED=6

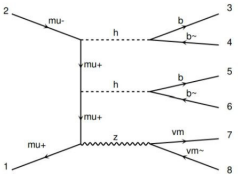

diagram 27 QCD=0, QED=6

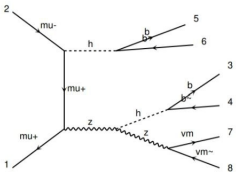

diagram 28 QCD=0, QED=6

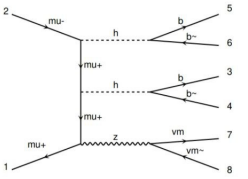

diagram 29 QCD=0, QED=6

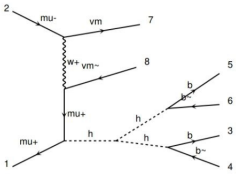

diagram 30 QCD=0, QED=6

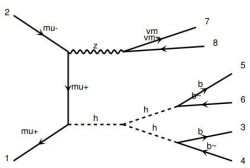

diagram 31 QCD=0, QED=6

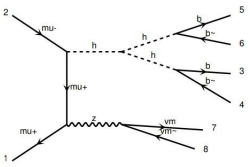

diagram 32 QCD=0, QED=6

- $\mu^+\mu^- \to W^+\, W^-\, \nu_\mu\, \overline{\nu}_\mu\ ,\ W^- \to d\, \overline{u}$

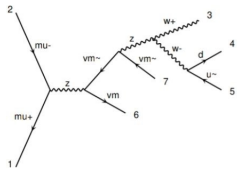

diagram 1 QCD=0, QED=5

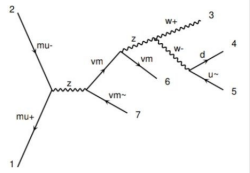

diagram 2 QCD=0, QED=5

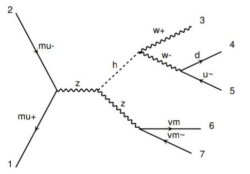

diagram 3 QCD=0, QED=5

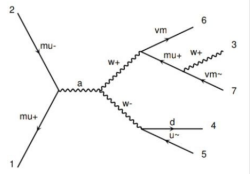

diagram 4 QCD=0, QED=5

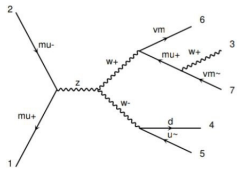

diagram 5 QCD=0, QED=5

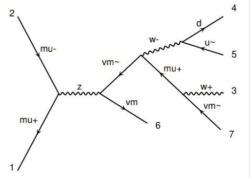

diagram 6 QCD=0, QED=5

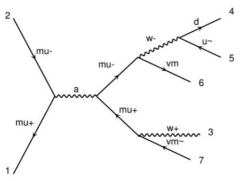

diagram 7 QCD=0, QED=5

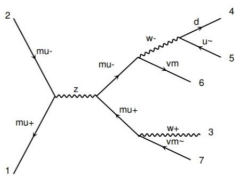

diagram 8 QCD=0, QED=5

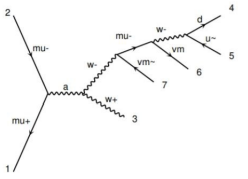

diagram 9 QCD=0, QED=5

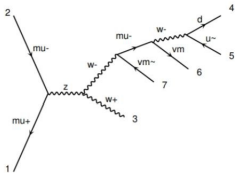

diagram 10 QCD=0, QED=5

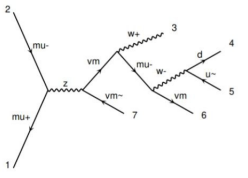

diagram 11 QCD=0, QED=5

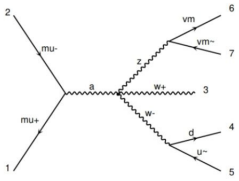

diagram 12 QCD=0, QED=5

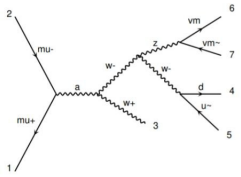

diagram 13 QCD=0, QED=5

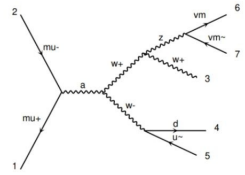

diagram 14 QCD=0, QED=5

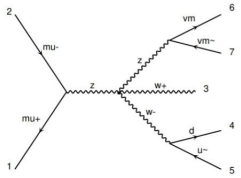

diagram 15 QCD=0, QED=5

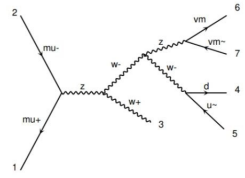

diagram 16 QCD=0, QED=5

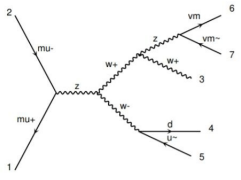

diagram 17 QCD=0, QED=5

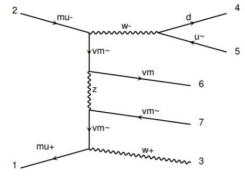

diagram 18 QCD=0, QED=5

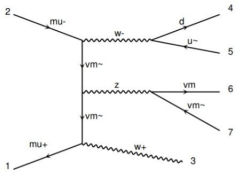

diagram 19 QCD=0, QED=5

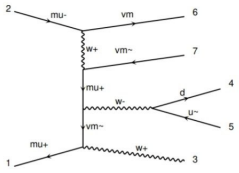

diagram 20 QCD=0, QED=5

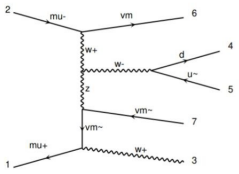

diagram 21 QCD=0, QED=5

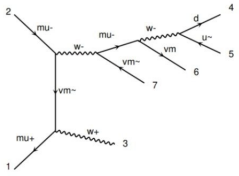

diagram 22 QCD=0, QED=5

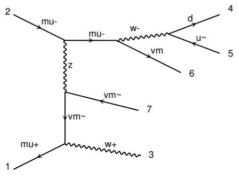

diagram 23 QCD=0, QED=5

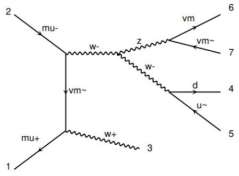

diagram 24 QCD=0, QED=5

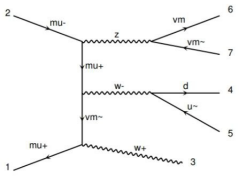

diagram 25 QCD=0, QED=5

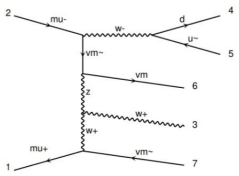

diagram 26 QCD=0, QED=5

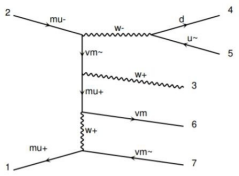

diagram 27 QCD=0, QED=5

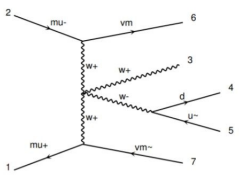

diagram 28 QCD=0, QED=5

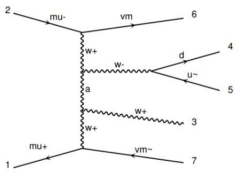

diagram 29 QCD=0, QED=5

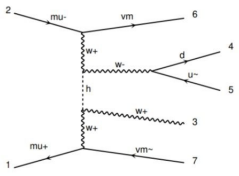

diagram 30 QCD=0, QED=5

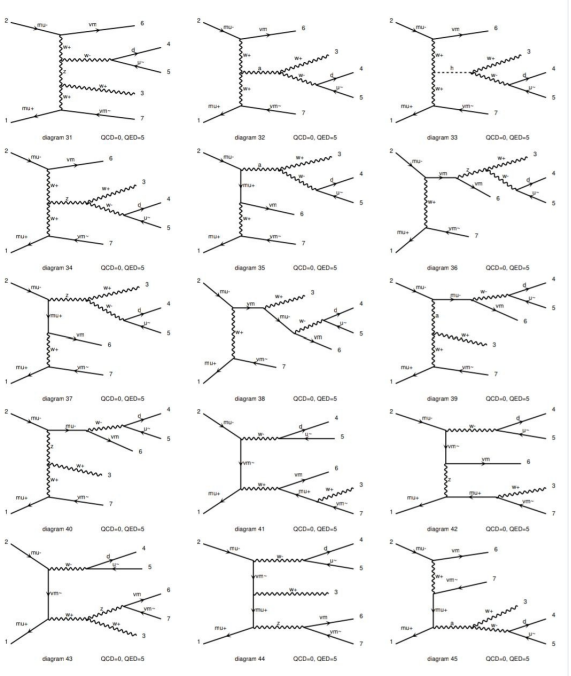

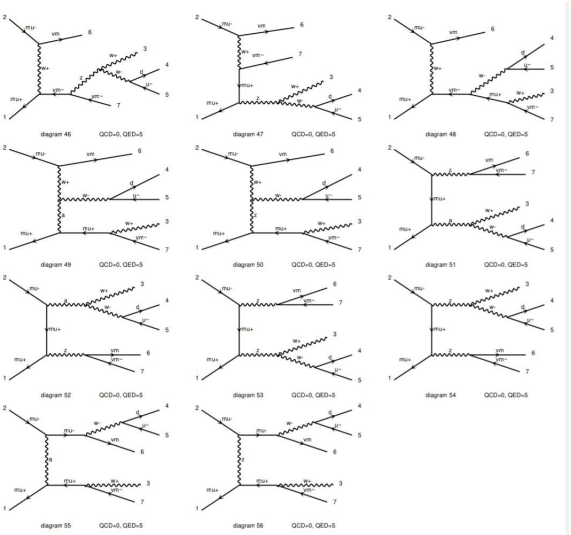

- $\mu^+\mu^- \to W^+\, W^-\, \nu_\mu\, \overline{\nu}_\mu\ ,\ W^- \to s\, \overline{c}$

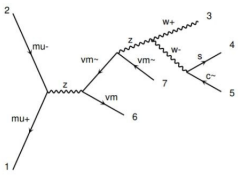

diagram 1 QCD=0, QED=5

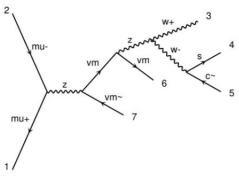

diagram 2 QCD=0, QED=5

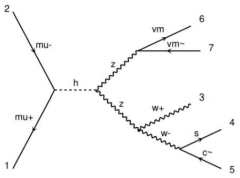

diagram 3 QCD=0, QED=5

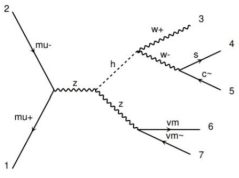

diagram 4 QCD=0, QED=5

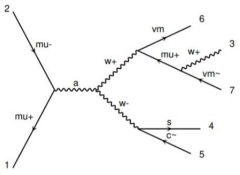

diagram 5 QCD=0, QED=5

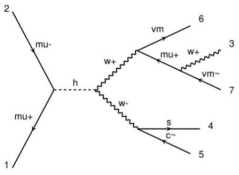

diagram 6 QCD=0, QED=5

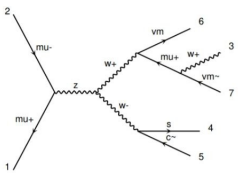

diagram 7 QCD=0, QED=5

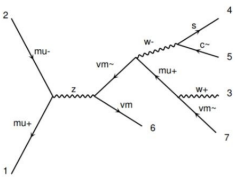

diagram 8 QCD=0, QED=5

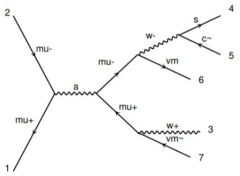

diagram 9 QCD=0, QED=5

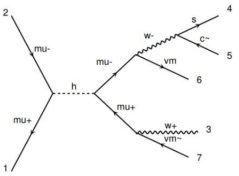

diagram 10 QCD=0, QED=5

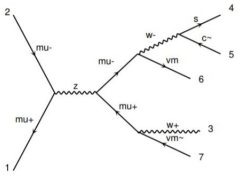

diagram 11 QCD=0, QED=5

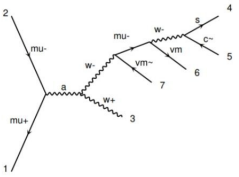

diagram 12 QCD=0, QED=5

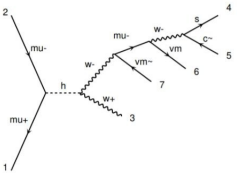

diagram 13 QCD=0, QED=5

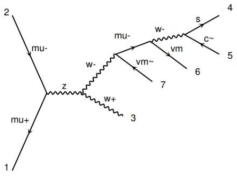

diagram 14 QCD=0, QED=5

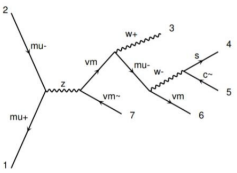

diagram 15 QCD=0, QED=5

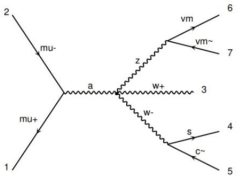

diagram 16 QCD=0, QED=5

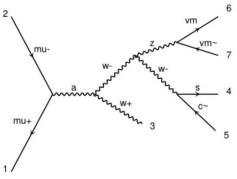

diagram 17 QCD=0, QED=5

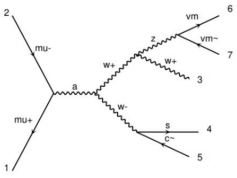

diagram 18 QCD=0, QED=5

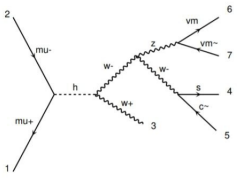

diagram 19 QCD=0, QED=5

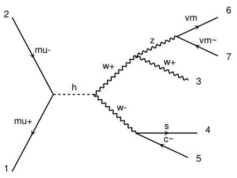

diagram 20 QCD=0, QED=5

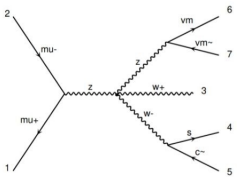

diagram 21 QCD=0, QED=5

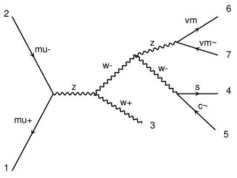

diagram 22 QCD=0, QED=5

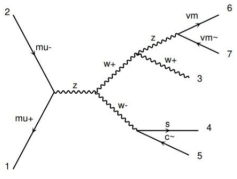

diagram 23 QCD=0, QED=5

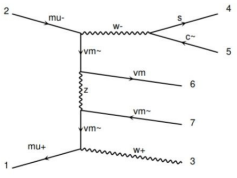

diagram 24 QCD=0, QED=5

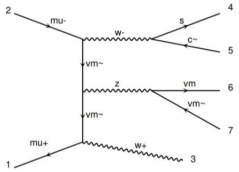

diagram 25 QCD=0, QED=5

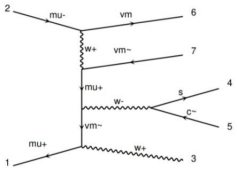

diagram 26 QCD=0, QED=5

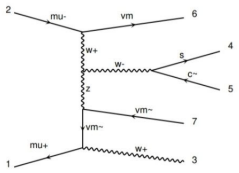

diagram 27 QCD=0, QED=5

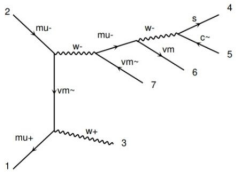

diagram 28 QCD=0, QED=5

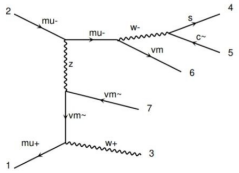

diagram 29 QCD=0, QED=5

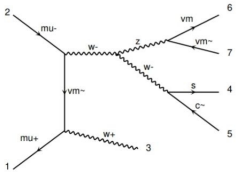

diagram 30 QCD=0, QED=5

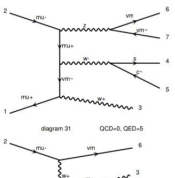

diagram 31 QCD=0, QED=5

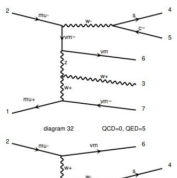

diagram 32 QCD=0, QED=5

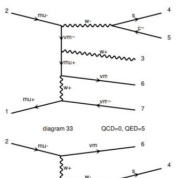

diagram 33 QCD=0, QED=5

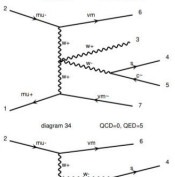

diagram 34 QCD=0, QED=5

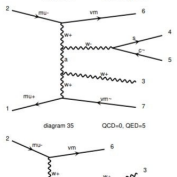

diagram 35 QCD=0, QED=5

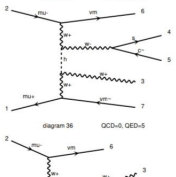

diagram 36 QCD=0, QED=5

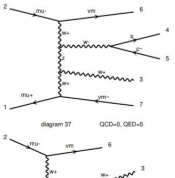

diagram 37 QCD=0, QED=5

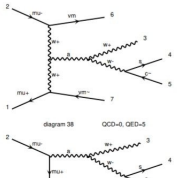

diagram 38 QCD=0, QED=5

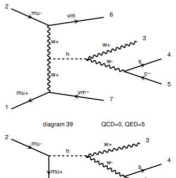

diagram 39 QCD=0, QED=5

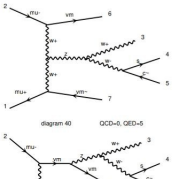

diagram 40 QCD=0, QED=5

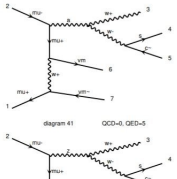

diagram 41 QCD=0, QED=5

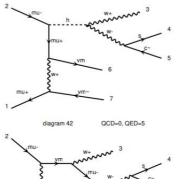

diagram 42 QCD=0, QED=5

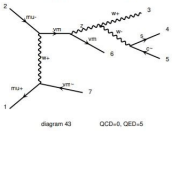

diagram 43 QCD=0, QED=5

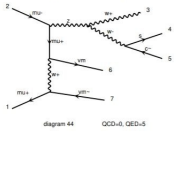

diagram 44 QCD=0, QED=5

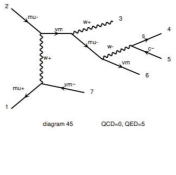

diagram 45 QCD=0, QED=5

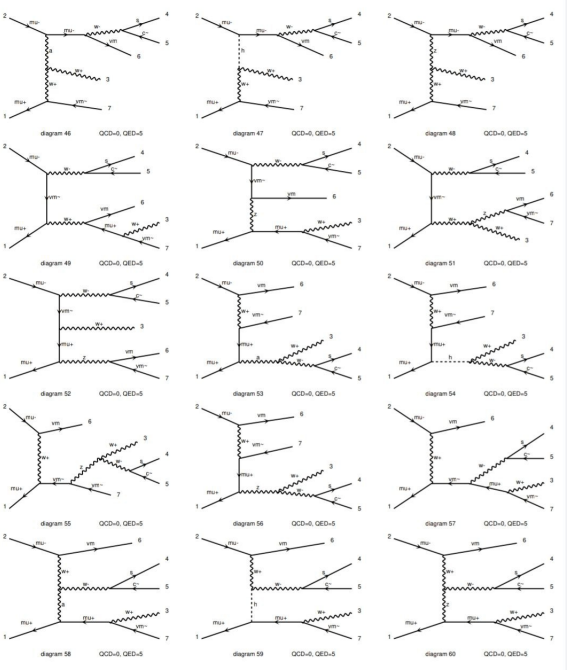
diagram 46 QCD=0, QED=5
diagram 47 QCD=0, QED=5
diagram 48 QCD=0, QED=5
diagram 49 QCD=0, QED=5
diagram 50 QCD=0, QED=5
diagram 51 QCD=0, QED=5
diagram 52 QCD=0, QED=5
diagram 53 QCD=0, QED=5
diagram 54 QCD=0, QED=5
diagram 55 QCD=0, QED=5
diagram 56 QCD=0, QED=5
diagram 57 QCD=0, QED=5
diagram 58 QCD=0, QED=5
diagram 59 QCD=0, QED=5
diagram 60 QCD=0, QED=5

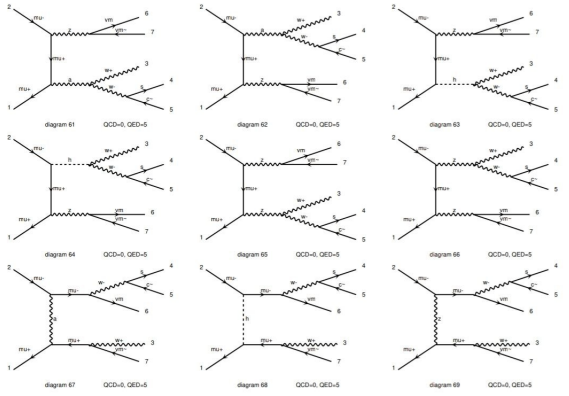
diagram 61 QCD=0, QED=5
diagram 62 QCD=0, QED=5
diagram 63 QCD=0, QED=5
diagram 64 QCD=0, QED=5
diagram 65 QCD=0, QED=5
diagram 66 QCD=0, QED=5
diagram 67 QCD=0, QED=5
diagram 68 QCD=0, QED=5
diagram 69 QCD=0, QED=5

Appendix 2

Here there are plots of energy, PT, θ and φ of charged particles in final state for single Higgs process.

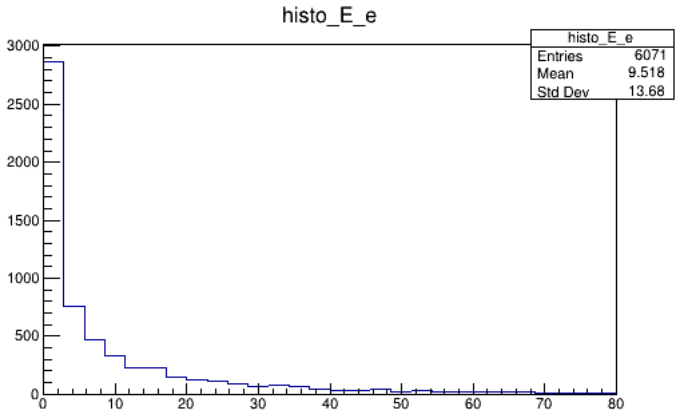

Figure 19: Energy distribution of electrons.

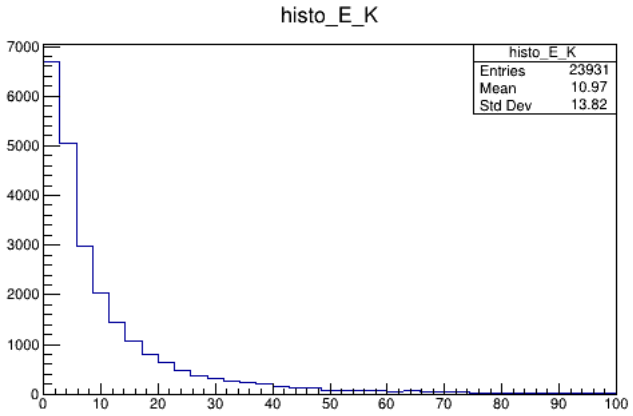

Figure 20: Energy distribution of kaons.

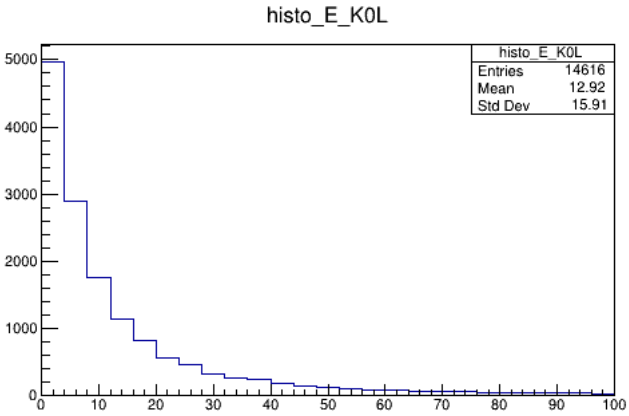

Figure 21: Energy distribution of long kaons.

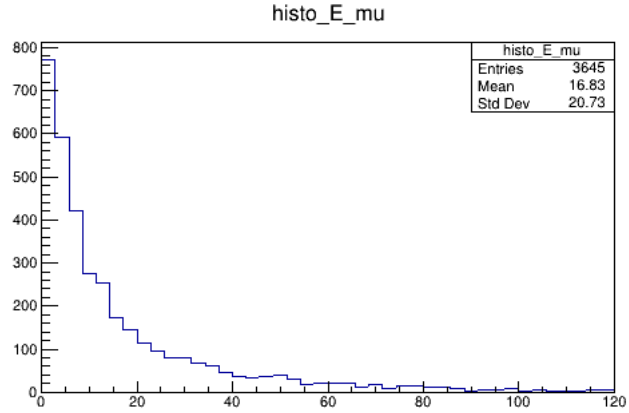

Figure 22: Energy distribution of muons.

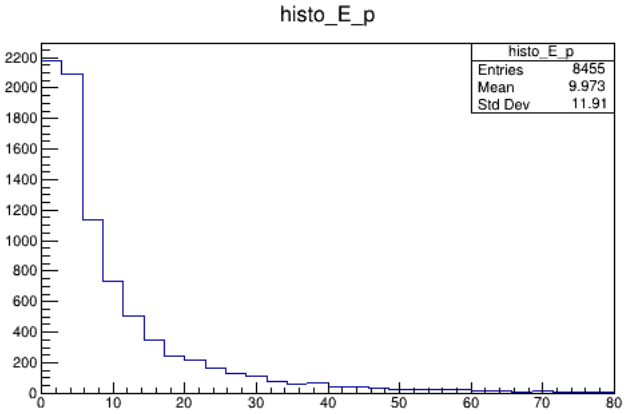

Figure 23: Energy distribution of protons.

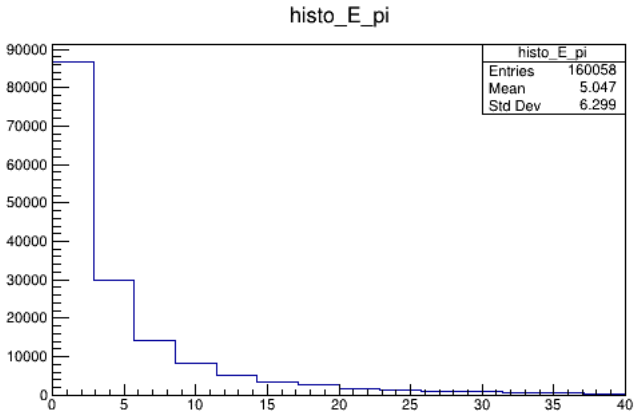

Figure 24: Energy distribution of pions.

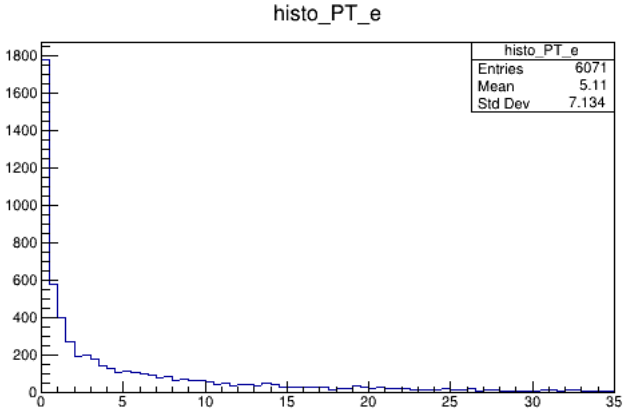

Figure 25: PT distribution of electrons.

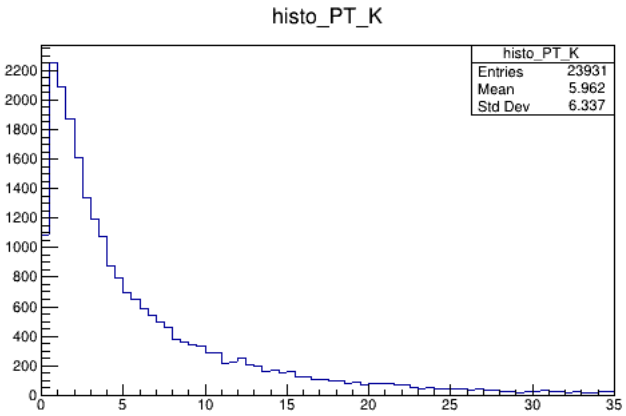

Figure 26: PT distribution of kaons.

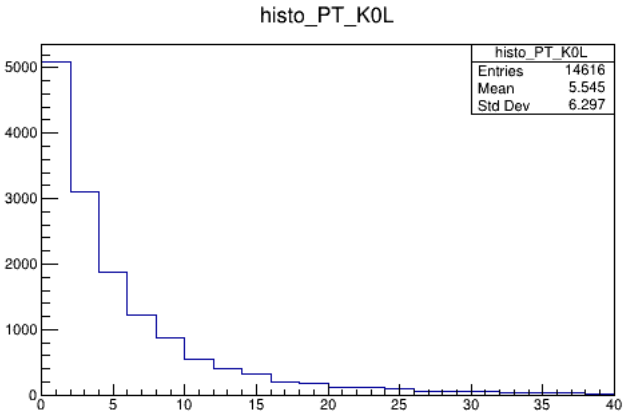

Figure 27: PT distribution of long kaons.

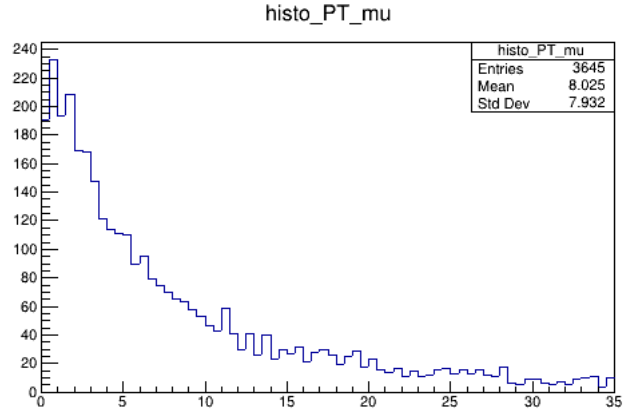

Figure 28: PT distribution of muons.

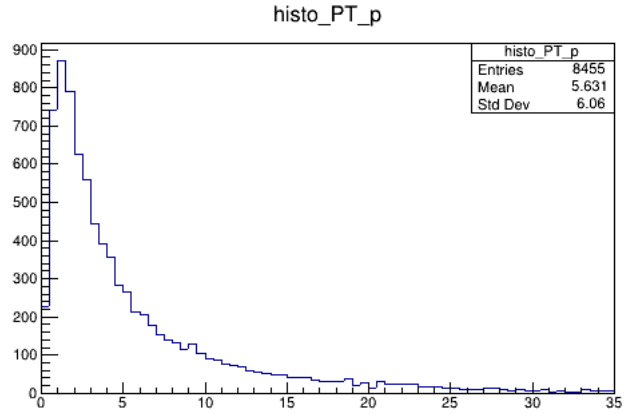

Figure 29: PT distribution of protons.

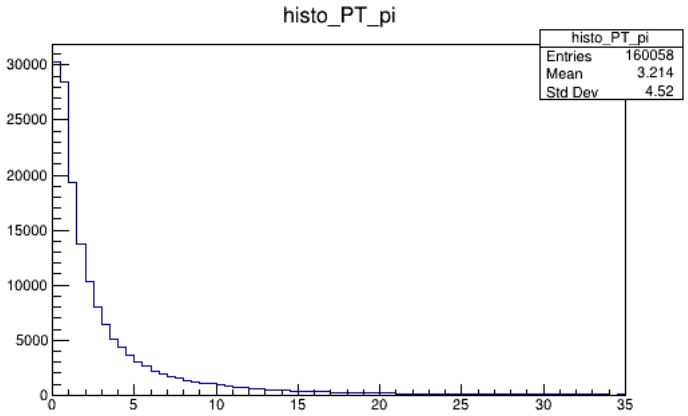

Figure 30: PT distribution of pions.

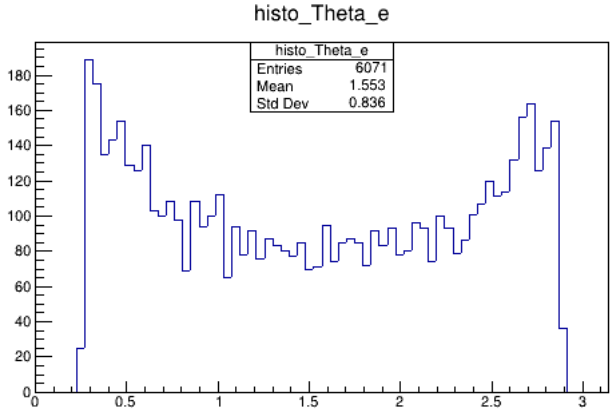

Figure 31: θ distribution of electrons.

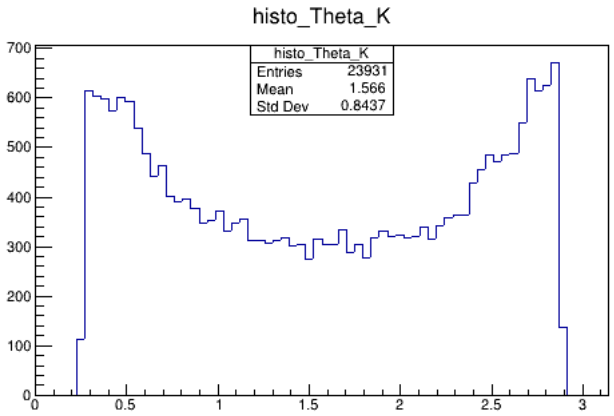

Figure 32: θ distribution of kaons.

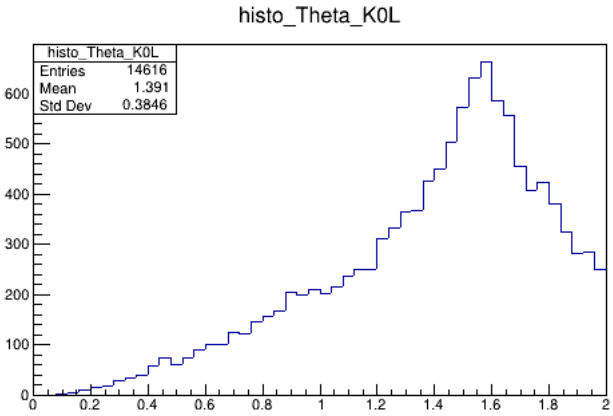

Figure 33: θ distribution of long kaons.

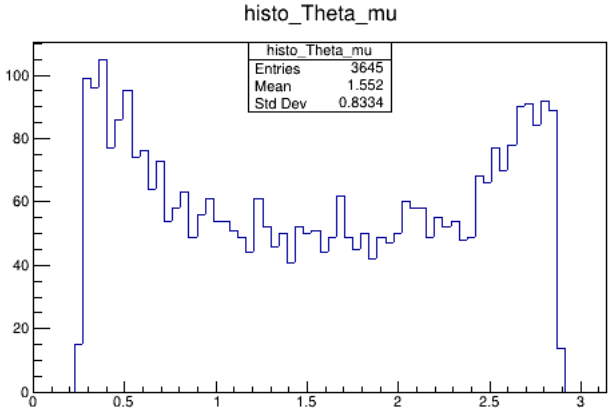

Figure 34: θ distribution of muons.

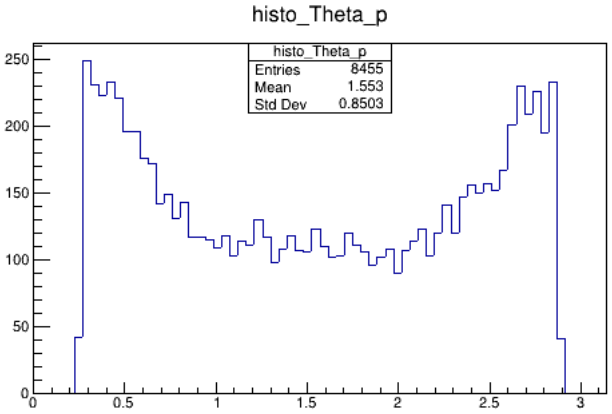

Figure 35: θ distribution of protons.

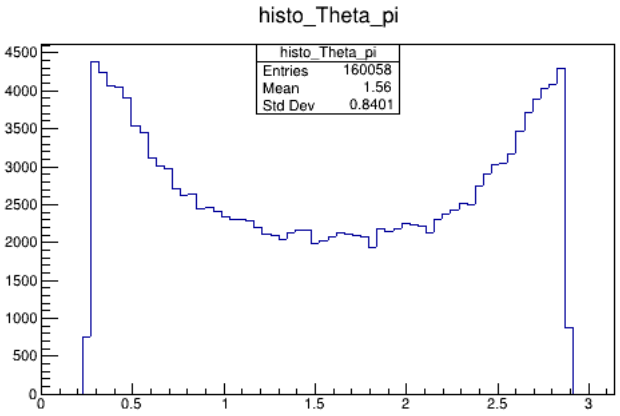

Figure 36: θ distribution of pions.

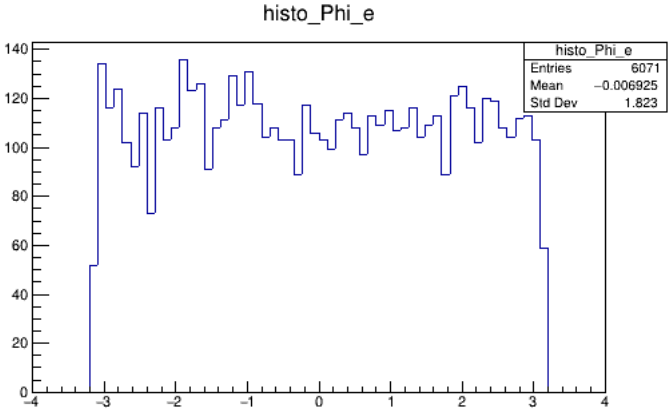

Figure 37: φ distribution of electrons.

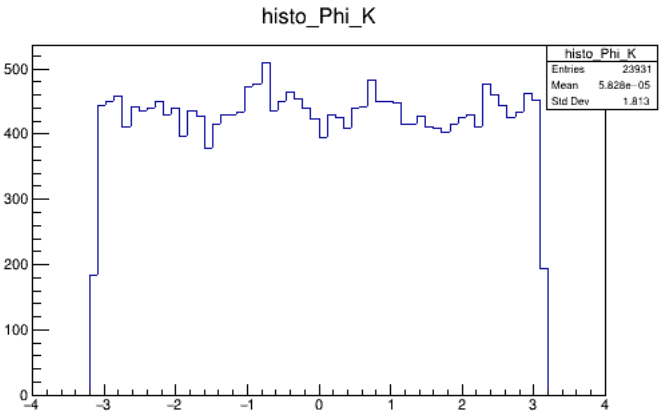

Figure 38: φ distribution of kaons.

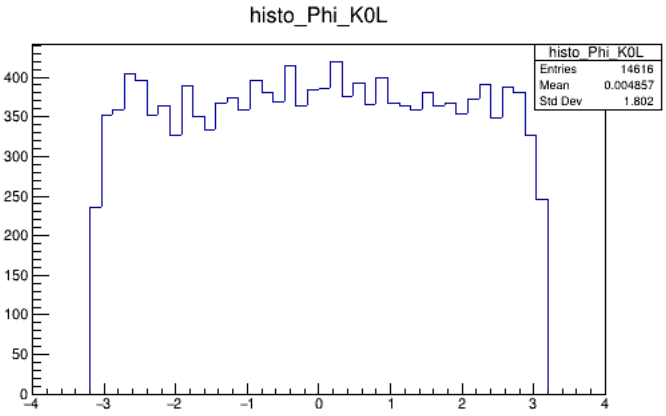

Figure 39: φ distribution of long kaons.

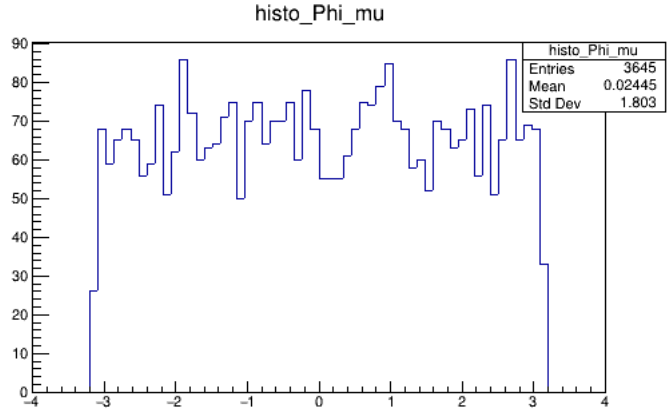

Figure 40: φ distribution of muons.

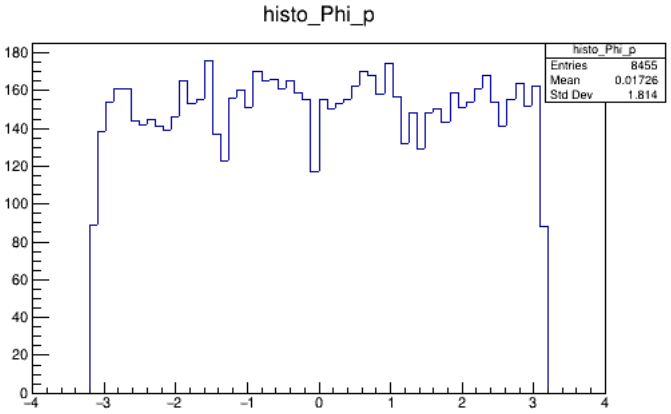

Figure 41: φ distribution of protons.

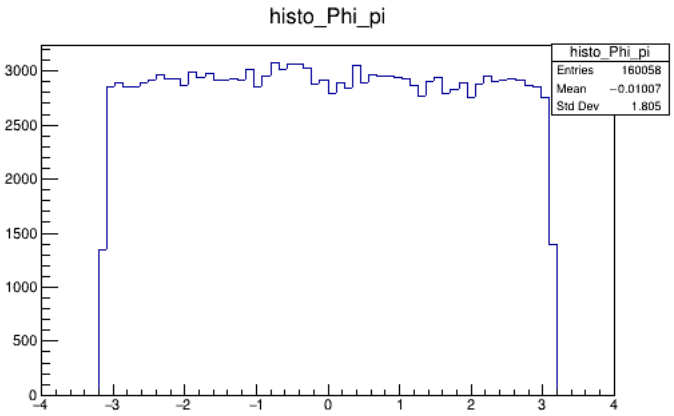

Figure 42: φ distribution of pions.

References

[1] K.M. Black, S. Jindariani, D. Li, F. Maltoni, P. Meade, D. Stratakis, *Muon Collider Forum Report*, 2022.

[2] J.P. Delahaye, et al., *Muon colliders*, arXiv:1901.06150, 2019.

[3] K. R. Long, D. Lucchesi, M. A. Palmer, N. Pastrone, D. Schulte and V. Shiltsev, *Muon colliders to expand frontiers of particle physics*, Nature Physics, VOL 17, Marzo 2021.

[4] P.A. Zyla et al. (Particle Data Group), *The Review of Particle Physics*, Prog. Theor. Exp. Phys. 2020, 083C01 (2020).

[5] C. Aimè, et al, *Simulated Detector Performance at the Muon Collider*, 2022.

[6] Francesco Collamati, et al, *Advanced Assessment of Beam-Induced Background at a Muon Collider*, arxiv eprint: R1PUNPY11V, 2021.

[7] Muon Collider Detector Design and Performance Group, *Muon Collider Detector.* https://muoncollider.web.cern.ch/design/muon-collider-detector, 2021. [Last checked: 13-october-2021].

[8] J. Alwall et al., *The automated computation of tree-level and next-to-leading order differential cross sections, and their matching to parton shower simulations*, Journal of High Energy Physics, vol. 2014, no. 7, pp. 1–157, 2014.

[9] T. Sjöstrand et al., *An introduction to PYTHIA 8.2*, Computer physics communications, vol. 191, pp. 159–177, 2015.

[10] R. Brun, F. Rademakers, *ROOT - An Object Oriented Data Analysis Framework*, Proceedings AIHENP '96 Workshop, Lausanne, Sep. 1996, Nucl. Inst. & Meth. in Phys. Res. A 389 (1997) '81-'86.